# **NJC**



**View Article Online PAPER** 



Cite this: New J. Chem., 2019, **43**, 3719

Received 12th December 2018, Accepted 28th January 2019

DOI: 10.1039/c8nj06270f

rsc.li/njc

# Metal-cation substitutions induced the enhancement of second harmonic generation in $A_8BS_6$ (A = Cu, and Aq; B = Si, Ge, and Sn)†

Le Gao, Ming-Hsien Leeb and Jun Zhang \*\*

Screening a good-performance infrared (IR) nonlinear optical (NLO) material with a large band gap, appropriate second harmonic generation (SHG) response and moderate birefringence has inspired the study of  $A_8BS_6$  (A = Cu, and Ag; B = Si, Ge, and Sn). The  $A_8BS_6$  series exhibits apparently hierarchical changes in the optical properties with ion-substitution under the same symmetry. In this paper, by the first-principles method and SHG-density method, the electronic structure, the optical properties and the contribution of respective ions and ion groups have been investigated. This reveals that the substitution from Ag to Cu with isostructural compounds induces the apparent enhancement of the SHG responses, which is mainly attributed to the different intensity of dp hybridization between the A cation and S. In addition, tetrahedra formed by B-site cations contribute little to the SHG, mainly because they offset each other. For the tiny changes in band gaps, it is found that the synergetic effect of B-site ion size, compound volume size and dp hybridization of A-S plays an important role. This study provides a feasible way to design and synthesize good-performance IR NLO materials.

### Introduction

Since the laser and second harmonic generation (SHG) were discovered, second-order nonlinear optical (NLO) materials have been widely used in scientific and technological fields, including visible laser generation, artificial nuclear fusion, precision scientific instruments, and so on. 1-4 In the past few decades, lots of well-known materials applied in the ultraviolet (UV) region have been synthesized such as KH<sub>2</sub>PO<sub>4</sub> (KDP),<sup>5,6</sup> KTiOPO<sub>4</sub> (KTP), <sup>7</sup> β-Ba<sub>2</sub>BO<sub>4</sub> (BBO), <sup>8</sup> LiB<sub>3</sub>O<sub>5</sub> (LBO)<sup>9</sup> and KBe<sub>2</sub>BOF<sub>2</sub> (KBBF). 10-12 Recently, also springing-up, CsB<sub>4</sub>O<sub>6</sub>F, 13 NH<sub>4</sub>B<sub>4</sub>O<sub>6</sub>F, 14  $LiB_6O_9F_1^{15}K_3B_6O_{10}Cl_1^{16}Pb_2Ba_3(BO_3)_3Cl_1^{17}$  and  $AB_4O_6F$  (A = K, Rb, and Cs)18 have become some of the new deep-UV candidates.

In the mid/far IR region, well-known NLO materials such as AgGaQ<sub>2</sub> (Q = S, and Se) and ZnGeP<sub>2</sub> (ZGP) are commercially used. They possess high SHG coefficients of about 13 pm V<sup>-1</sup>, 33 pm V<sup>-1</sup>, and 75 pm V<sup>-1</sup>, respectively. 10 Despite the large NLO coefficients, these materials have disadvantages that hinder their application in mid-IR laser generation, for example, the value of laser damage threshold (LDT) for AgGaS<sub>2</sub><sup>19</sup> and AgGaSe<sub>2</sub><sup>20</sup>

is very small and only reaches 2 W cm<sup>-1</sup> and 11 MW cm<sup>-1</sup>, (@1.06 μm, 35 ns), respectively. 10

As we all know, metal chalcogenides can be used in the mid/far IR region. Comparing metal chalcogenides with oxides, the weaker electronegativity difference in metal chalcogenides will lead to a red shift to expand the transparency, therefore the relationship between microscopic structure and macroscopic properties will be different from oxides. It is known that the larger band gap may be beneficial in generating high LDTs, but results in small NLO coefficients. In the IR region, good NLO materials should have a large energy band gap ( $\geq 3.0$  eV) and moderate SHG response (comparable to AgGaS<sub>2</sub>). Balancing the large energy band gap and appropriate SHG response has been a challenge for a long time.21,22 The Ag-containing and Cu-containing chalcogenides are recognized as important NLO crystals in the IR region. Except for AgGaS2, AgGaSe2 and CuGaS<sub>2</sub>, many Ag and Cu chalcogenides have been synthesized:  $AgHoSe_2$ ,  $Ag_2In_2MS_6$  (M = Si, and Ge),  $AgCd_2GaS_4$ ,  $Ag_2BaGeSe_4$ , Ag<sub>2</sub>BaSnSe<sub>4</sub>, Ag<sub>2</sub>BaSiSe<sub>4</sub>, Ag<sub>2</sub>CdSnS<sub>4</sub>, Cu<sub>2</sub>BaSiSe<sub>4</sub>, Cu<sub>2</sub>BaGeS<sub>4</sub>, Cu<sub>2</sub>BaGeSe<sub>4</sub>, Cu<sub>2</sub>BaSnS<sub>4</sub> and Cu<sub>2</sub>BaSnSe<sub>4</sub>.<sup>23,24</sup> As is common knowledge, Ag-containing and Cu-containing compounds have relatively large SHG responses but relatively small gaps, for instance,  $AgGaGeS_4$  ( $E_g = 2.53$  eV, 15.0 pm  $V^{-1}$ ),  $Ag_2BaGeS_4$  $(E_{\rm g} = 2.02 \text{ eV}, 22.1 \text{ pm V}^{-1})$ , and  $Cu_2BaSnS_4$   $(E_{\rm g} = 1.96 \text{ eV},$ 20.0 pm  $V^{-1}$ ). 23,24 One may notice that there are still Agcontaining compounds with large gaps: AgGaGeS<sub>4</sub> ( $E_g$  = 3 eV) and  $KAg_2PS_4$  ( $E_g = 3.02$  eV). So, this raises the question, what

<sup>&</sup>lt;sup>a</sup> School of Physics Science and Technology, Xinjiang University, Urumqi, Xinjiang 830046, China. E-mail: zhangjunxju@163.com

<sup>&</sup>lt;sup>b</sup> Department of Physics, Tamkang University, New Taipei 25137, Taiwan

<sup>†</sup> Electronic supplementary information (ESI) available: Band structures, local dipole moment calculation, birefringence Mulliken population, ionic radii, bond length and volume for Cu<sub>8</sub>SiS<sub>6</sub>, Cu<sub>8</sub>GeS<sub>6</sub>, Ag<sub>8</sub>GeS<sub>6</sub>, and Ag<sub>8</sub>SnS<sub>6</sub>. See DOI: 10.1039/ c8nj06270f

Paper NJC

kind of Ag-containing compounds may have a large gap without loss of a large SHG response and what is the origin of these properties. In this paper, we focus on four Ag-containing and Cu-containing compounds, Cu<sub>8</sub>SiS<sub>6</sub>,<sup>25</sup> Cu<sub>8</sub>GeS<sub>6</sub>,<sup>26</sup> Ag<sub>8</sub>GeS<sub>6</sub><sup>27</sup> and Ag<sub>8</sub>SnS<sub>6</sub>.<sup>28</sup> Cu<sub>8</sub>SiS<sub>6</sub> was first reported by PAR M. et al. in 1981. Cu<sub>8</sub>GeS<sub>6</sub> was first synthesised by M. Ishii et al. in 1999. Ag<sub>8</sub>GeS<sub>6</sub> and Ag<sub>8</sub>SnS<sub>6</sub> were first researched by Wang, N.<sup>29</sup> et al. in 1978. However, their nonlinear effects vary widely, and their intrinsic response mechanisms have not been reported. In this work, the electronic structure and optical properties are estimated by a combination of the density functional theory (DFT), SHG-density and band-resolved methods, and the results show that the intensity of dp hybridization between d<sup>10</sup> cation and S has an important influence on the SHG responses, which clarifies the origin of the apparent enhancement of the SHG responses caused by the substitution from Ag to Cu.

### Calculation method

All the compounds crystalize in an orthogonal manner and have non-centrosymmetric (NCS) structures. The first-principles calculations were performed by the plane wave pseudopotential method implemented in the CASTEP package.30 During the calculation, we adopted the generalized gradient approximation (GGA) and Perdew-Burke-Ernzerhof (PBE) functional.31 The norm-conserving pseudopotential (NCP)32,33 was set up to calculate the electronic structure and optical properties. The energy cutoff was set to 880 eV for Ag<sub>8</sub>GeS<sub>6</sub>, Ag<sub>8</sub>SnS<sub>6</sub>, Cu<sub>8</sub>SiS<sub>6</sub> and Cu<sub>8</sub>GeS<sub>6</sub> to reach the convergence of calculation. The following orbital electrons were treated as valence electrons: S 3s<sup>2</sup>3p<sup>4</sup>, Ag  $4s^24p^64d^{10}5s^1$ , Ge  $4s^24p^2$ , Cu  $3d^{10}4s^1$ , and Si  $3s^23p^2$ , and the Brillouin zone was performed using a 2  $\times$  4  $\times$  3 (for Ag<sub>8</sub>GeS<sub>6</sub> and  $Ag_8SnS_6$ ) and  $4 \times 4 \times 3$  (for  $Cu_8GeS_6$  and  $Cu_8SiS_6$ ) Monkhorst-Pack k-point sampling, respectively. When using the CASTEP code for calculation, we kept the default values of related calculation parameters and convergent criteria.

In order to further elucidate the microscopic origins of the optical properties, the SHG response was estimated through calculating the second-order NLO coefficients at zero frequency limit. The formula of second-order coefficients can be derived as:<sup>34</sup>

$$\chi_{\alpha\beta\gamma} = \chi_{\alpha\beta\gamma} \text{ (VE)} + \chi_{\alpha\beta\gamma} \text{ (VH)}.$$

And,

$$\begin{split} \chi^{\alpha\beta\gamma}(\mathrm{VH}) &= \frac{e^3}{2\hbar^2 m^3} \sum_{\mathrm{vv'c}} \int & \frac{d^3k}{4\pi^3} p(\alpha\beta\gamma) \mathrm{Im} \left[ p_{\mathrm{vv'}}^{\alpha} p_{\mathrm{v'c}}^{\beta} p_{\mathrm{cv}}^{\gamma} \right] \\ &\times \left( \frac{1}{\omega_{\mathrm{cv}}^3 \omega_{\mathrm{v'c}}^2} + \frac{1}{\omega_{\mathrm{cv}}^4 \omega_{\mathrm{v'c}}} \right) \end{split}$$

$$\begin{split} \chi^{\alpha\beta\gamma}(\mathrm{VE}) &= \frac{e^3}{2\hbar^2 m^3} \sum_{\mathrm{vcc'}} \int & \frac{d^3k}{4\pi^3} p(\alpha\beta\gamma) \mathrm{Im} \left[ p_{\mathrm{vc}}^{\alpha} p_{\mathrm{cc'}}^{\beta} p_{\mathrm{c'}}^{\gamma} \right] \\ & \times \left( \frac{1}{\omega_{\mathrm{cv}}^3 \omega_{\mathrm{cv'}}^2} + \frac{1}{\omega_{\mathrm{ev}}^4 \omega_{\mathrm{vc'}}} \right) \end{split}$$

where  $\alpha$ ,  $\beta$ , and  $\gamma$  are Cartesian components, v and v' denote valence bands, c and c' refer to conduction bands, and  $p(\alpha\beta\gamma)$  denotes full permutation. The band energy difference and momentum matrix elements are denoted as  $\hbar\omega_{ij}$  and  $p_{ij}^{\alpha}$ , respectively.

### Crystal structure

Although all title compounds have the similar formula A<sub>8</sub>BC<sub>6</sub>, they crystallize in different polar space groups. Among them, Cu<sub>8</sub>SiS<sub>6</sub> and Cu<sub>8</sub>GeS<sub>6</sub> belong to the space group *Pmn*2<sub>1</sub> of the orthogonal system, Ag<sub>8</sub>GeS<sub>6</sub> and Ag<sub>8</sub>SnS<sub>6</sub> crystalize in *Pna*2<sub>1</sub> of the orthogonal system. Additionally, even though the element substitution (Cu to Ag, Ge to Si and Ge to Sn) in the A<sub>8</sub>BC<sub>6</sub> family is simple, they show an obvious structural transformation from *Pmn*2<sub>1</sub> to *Pna*2<sub>1</sub>. All the structures demonstrate a three – dimensional (3D) framework, and here we take Cu<sub>8</sub>SiS<sub>6</sub> and Ag<sub>8</sub>GeS<sub>6</sub> as examples to describe the crystal structures (shown in Fig. 1). The detailed crystallographic information of the title compounds is listed in the ESI† Table S1.

In  $Cu_8SiS_6$ , Z = 2 (number of molecules in a unit cell), there are sixteen Cu atoms, two Si atoms and twenty S atoms in a unit cell; the Cu atoms have two types of coordination: distorted tetrahedral  $[CuS_4]$  units and flat triangular  $[CuS_3]$  units. (Fig. 1).

In  $Ag_8GeS_6$ , Z=4, its unit cell contains four Ge atoms, thirty two Ag atoms and twenty four S atoms. The structure (shown in Fig. 1) is complex. It clearly shows that Ag has three kinds of coordination, distorted tetrahedral  $[AgS_4]$  units, flat triangular  $[AgS_3]$  and linear  $[AgS_2]$  units. Thus, the structure is formed by  $[GeS_4]$ ,  $[AgS_4]$  tetrahedron and  $[AgS_3]$  triangles through sharing S atoms; Ag atoms with linear coordination are additionally introduced into the voids of this carcass (Table 1).<sup>27</sup>

# Band gap and electronic structure

A plane-wave pseudopotential CASTEP package based on DFT was employed to provide the description of band structures and

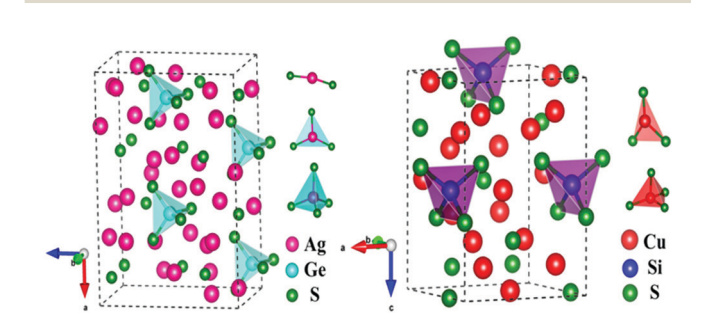


Fig. 1 Crystallographic structures of Cu<sub>8</sub>SiS<sub>6</sub> and Ag<sub>8</sub>GeS<sub>6</sub>

 Table 1
 Crystallographic structure data of the title compounds

Compound	Cu <sub>8</sub> SiS <sub>6</sub>	Cu <sub>8</sub> GeS <sub>6</sub>	Ag <sub>8</sub> GeS <sub>6</sub>	Ag <sub>8</sub> SnS <sub>6</sub>
Crystal system Space group a (Å) b (Å) c (Å)	Orthogonal Pmn2 <sub>1</sub> 6.992 6.900 9.772	Orthogonal <i>Pmn2</i> <sub>1</sub> 7.044 6.966 9.869	Orthogonal <i>Pna2</i> <sub>1</sub> 15.13 7.46 10.58	Orthogonal <i>Pna</i> 2 <sub>1</sub> 15.298 7.548 10.699

NJC

Table 2 The calculated band gap and SHG tensors of Cu<sub>8</sub>SiS<sub>6</sub>, Cu<sub>8</sub>GeS<sub>6</sub>, Ag<sub>8</sub>GeS<sub>6</sub> and Ag<sub>8</sub>SnS<sub>6</sub>

Compound	Calculated SHG tensors $(pm V^{-1})$	Band gap (GGA + PBE)
Cu <sub>8</sub> SiS <sub>6</sub>	$d_{15} = 3.10$	0.97 (Cal.)
	$d_{24}$ = -9.62	1.30 (Exp.)
	$d_{33} = -8.13$	
Cu <sub>8</sub> GeS <sub>6</sub>	$d_{15}$ = 13.68	0.72 (Cal.)
	$d_{24} = 0.97$	_
	$d_{33} = 11.03$	
Ag <sub>8</sub> GeS <sub>6</sub>	$d_{15} = -1.85$	0.78 (Cal.)
	$d_{24} = -2.84$	1.45 (Exp.)
	$d_{33} = -4.98$	
Ag <sub>8</sub> SnS <sub>6</sub>	$d_{15} = 3.92$	0.55 (Cal.)
	$d_{24} = 0.65$	1.39 (Exp.)
	$d_{33} = 5.78$	

electronic structures.<sup>35</sup> The calculated band gaps are 0.97 eV for Cu<sub>8</sub>SiS<sub>6</sub>, 0.72 eV for Cu<sub>8</sub>GeS<sub>6</sub>, 0.78 eV for Ag<sub>8</sub>GeS<sub>6</sub>, and 0.55 eV for Ag<sub>8</sub>SnS<sub>6</sub>, respectively (shown in Table 2). The calculated band gap is slightly smaller than the experimental band gap, the underestimate of band gap is due to the discontinuity of energy of the GGA functional. Their band structures are qualitatively similar to one another and are direct band gaps (shown in Fig. S1, ESI†). To further elucidate the microscopic origins of the optical properties, the first-principles electronic structures of Cu<sub>8</sub>SiS<sub>6</sub>, Cu<sub>8</sub>GeS<sub>6</sub>, Ag<sub>8</sub>GeS<sub>6</sub> and Ag<sub>8</sub>SnS<sub>6</sub> were obtained and are shown in Fig. 2a-d. According to the total and partial density of states (PDOS) in Fig. 2a, we conclude that the energy level from -3.5 to 0 eV at the valence band maximum (VBM) is mainly contributed by Cu-4p4d and S-2p orbitals. The energy level from 2 to 5 eV at the conduction band minimum (CBM) is mainly dominated by Cu-4p and S-2p orbitals. As shown in Fig. 2(c), the contributions at the valence band maximum for Ag<sub>8</sub>GeS<sub>6</sub> are mainly from the S-2p orbital, the Ag-5s4p4d orbital and slightly from the Ge-4p orbital, the contributions to the conduction band are mainly from the Ge-4p, S-2p and Ag-5s4p orbitals. This indicates that the interaction between Cu-S in [CuS4] and [CuS<sub>3</sub>] has a more important influence on the band gaps of Cu<sub>8</sub>SiS<sub>6</sub> and Cu<sub>8</sub>GeS<sub>6</sub> than that of Si-S in [SiS<sub>4</sub>] or Ge-S in [GeS<sub>4</sub>]. Also, in Ag<sub>8</sub>GeS<sub>6</sub> and Ag<sub>8</sub>SnS<sub>6</sub>, the interactions between Ag-S in  $[AgS_4][AgS_3]$  and  $[AgS_2]$  determine the band gap.<sup>36</sup>

One may notice that the band gaps of Cu<sub>8</sub>SiS<sub>6</sub>, Cu<sub>8</sub>GeS<sub>6</sub>, Ag<sub>8</sub>GeS<sub>6</sub> and Ag<sub>8</sub>SnS<sub>6</sub> are apparently different although they are isostructural compounds to each other. Since the properties have a relation with the electron transition from the top of the valence bands to the bottom of the conduction bands near the Fermi level, to explore the differences among the band gaps, we calculated the orbitals and analysed the VBM and CBM (shown in Fig. 2).<sup>37</sup> It is clearly shown that the orbitals from the Cu atoms and S atoms dominate the VBM and CBM of Cu<sub>8</sub>SiS<sub>6</sub> and Cu<sub>8</sub>GeS<sub>6</sub>. The Ag atoms and S atoms contribute to the VBM and CBM of Ag<sub>8</sub>GeS<sub>6</sub> and Ag<sub>8</sub>SnS<sub>6</sub>, which is coincident with the results from the PDOS. To gain more insight on the difference of the band gaps, we performed Mulliken population analysis and ion size analysis (shown in Table S3, ESI†). The calculated results reveal that there is a trend of an increase in bond length from Cu<sub>8</sub>SiS<sub>6</sub> to Cu<sub>8</sub>GeS<sub>6</sub> and from Ag<sub>8</sub>GeS<sub>6</sub> to Ag<sub>8</sub>SnS<sub>6</sub>.

The volume of  $Cu_8SiS_6$  (471.517 Å<sup>3</sup>),  $Cu_8GeS_6$  (484.343 Å<sup>3</sup>),  $Ag_8GeS_6$  (1174.46 Å<sup>3</sup>), and  $Ag_8SnS_6$  (1235.41 Å<sup>3</sup>) also increased via the enlargement of the bond length. The ion size has an immediate influence on the electronic interactions between cation and anion orbitals. 38,39 Thus, the ionic radius of B-site  $Ge^{4+}$  (0.53 Å) is larger than that of B-site  $Si^{4+}$  (0.4 Å), which causes a stronger interaction with the anions (S), resulting in a broader Ge-2p orbital and the red shift of band gap in Cu<sub>8</sub>GeS<sub>6</sub> compared to Cu<sub>8</sub>SiS<sub>6</sub>. In Ag<sub>8</sub>GeS<sub>6</sub> and Ag<sub>8</sub>SnS<sub>6</sub>, the ionic radius of B-site  $\mathrm{Sn}^{4+}$  (0.69 Å) is larger than that of B-site  $\mathrm{Ge}^{4+}$  (0.53 Å), thus the broader Sn-2p orbital leads to the red shift of the band gap. That is why two compounds have the same structure but different band gaps. The changes in cell volume also offer an explanation for the variation in band gaps because the larger cell size will lead to a narrower energy level spacing and smaller band gap, 40 which is consistent with the conclusion drawn above.

The other reason that caused a smaller band gap is the difference of dp hybridization between A(A = Ag, Cu)-d and S-3p orbitals. 41 According to the PDOS (Fig. 2a and b), it is clear that the Cu-d orbital and S-3p orbital hybridize from -3 eV to the Fermi level at the top of the valence band; the dp hybridization is strong enough to affect the valence band energy shift and reduce the gap. In Ag<sub>8</sub>GeS<sub>6</sub> and Ag<sub>8</sub>SnS<sub>6</sub>, the situation is similar. As shown in Fig. 2c and d, the Ag-4d orbitals and S-3p orbitals hybridize from -2 eV to the Fermi level at the top of the valence band, the valence band energy will be also shifted, and hence the band gap is narrow in all title compounds.

### Optical properties

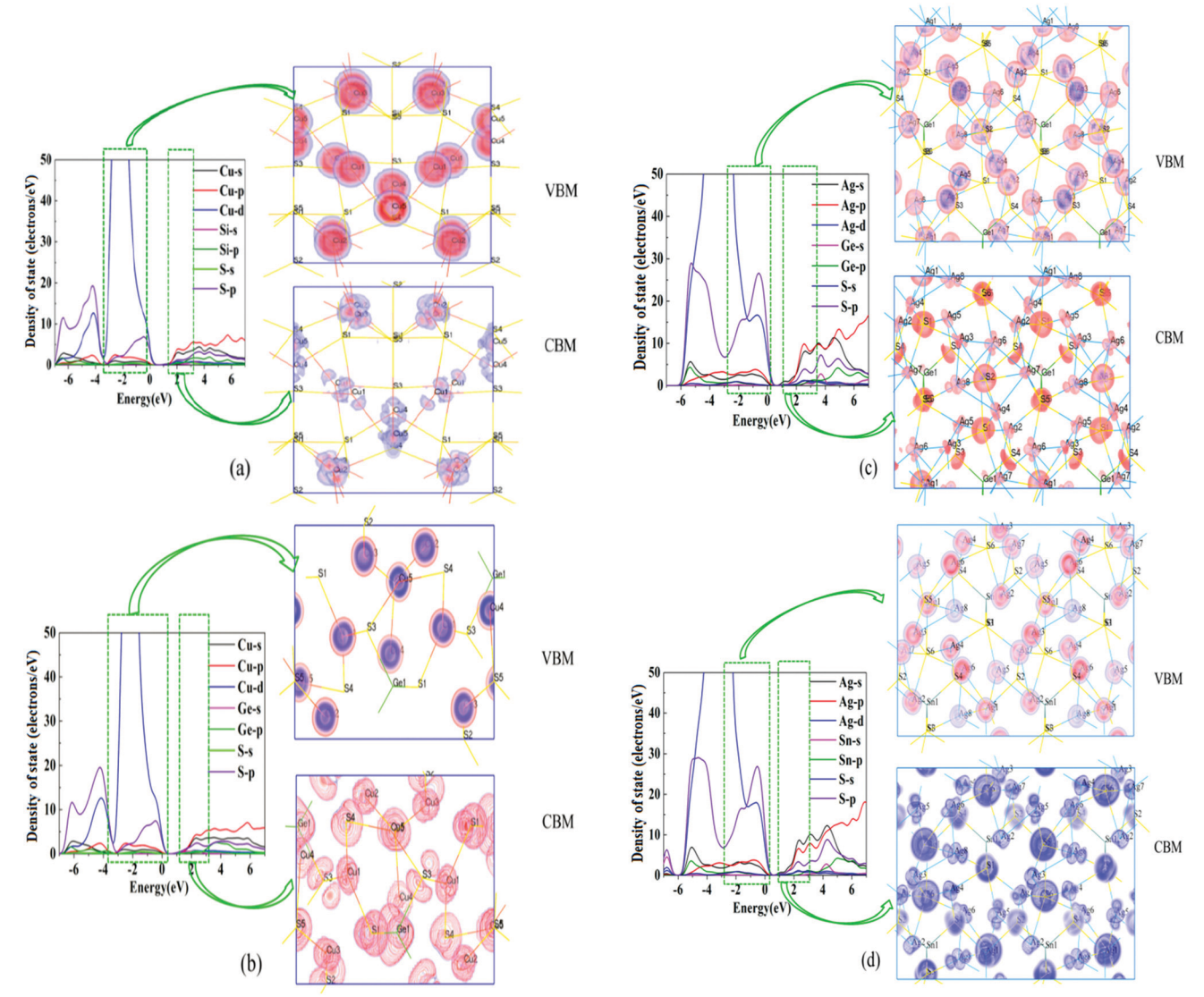
Using DFT, the dispersions of refractive indices in the static limit for Cu<sub>8</sub>SiS<sub>6</sub>, Cu<sub>8</sub>GeS<sub>6</sub>, Ag<sub>8</sub>GeS<sub>6</sub> and Ag<sub>8</sub>SnS<sub>6</sub> were obtained. The birefringences are 0.059 for Cu<sub>8</sub>SiS<sub>6</sub>, 0.080 for Cu<sub>8</sub>GeS<sub>6</sub>, 0.082 for Ag<sub>8</sub>GeS<sub>6</sub> and 0.095 for Ag<sub>8</sub>SnS<sub>6</sub> at 1064 nm (shown in Fig. S2, ESI†). The optical anisotropy is mainly attributed to the response electronic density distribution anisotropy (REDA) in SiS, GeS and SnS according to the REDA approximation proposed by Yang et al. 34,42 The moderate birefringence of all compounds proves that they are phase-matching materials.<sup>42</sup>

Considering that the calculation of SHG is highly sensitive to the band gap, a corrected scissors operator defined as the difference between the experimental gap and calculated gap was used when evaluating the calculated optical properties. 43 The calculated second order NLO coefficients are shown in Table 2. So, here, we will only discuss the largest effective SHG tensor of  $\text{Cu}_8\text{SiS}_6$  ( $d_{33} = -8.13 \text{ pm V}^{-1}$ ),  $\text{Cu}_8\text{GeS}_6$  ( $d_{33} = 11.03 \text{ pm V}^{-1}$ ),  $Ag_8GeS_6$  ( $d_{33} = -4.98 \text{ pm V}^{-1}$ ), and  $Ag_8SnS_6$  ( $d_{33} = 5.78 \text{ pm V}^{-1}$ ).

In order to analyse the contribution of an ion (or ionic group) to the SHG response, a SHG-density technique was adopted. It was performed by using the effective SHG of each band as a weighting coefficient to sum the probability densities of all states. SHG-density can be divided into occupied and unoccupied states of a virtual-electron (VE) and virtual-hole (VH), respectively. 40,44 The SHG-density caused by an ion can be clearly viewed through occupied and unoccupied states, however, the states that do not

Published on 29 January 2019. Downloaded by National Taiwan University on 3/29/2019 4:58:51 PM.

Paper



PDOS, VBM and CBM of Cu<sub>8</sub>SiS<sub>6</sub> (a), Cu<sub>8</sub>GeS<sub>6</sub> (b), Ag<sub>8</sub>GeS<sub>6</sub> (c) and Ag<sub>8</sub>SnS<sub>6</sub> (d)

contribute to the SHG response will be invisible. In Cu<sub>8</sub>GeS<sub>6</sub>, both the VH state and VE state have a positive effect on the effective SHG coefficient ( $d_{33}$ ); the VH state takes a dominant role, and the VE part plays a slight role (shown in Table 3). In Cu<sub>8</sub>SiS<sub>6</sub>, the VE state mainly dominates the effective SHG coefficient  $(d_{33})$ . Here, we show the VH of SHG-density for Cu<sub>8</sub>GeS<sub>6</sub> and the VE state for Cu<sub>8</sub>SiS<sub>6</sub> (shown in Fig. 3). In Cu<sub>8</sub>SiS<sub>6</sub> (Fig. 3a and b), Cu atoms mainly contribute to the occupied states. In the unoccupied states, the S atoms are the dominant

Table 3 The calculated largest effective SHG tensors of Cu<sub>8</sub>SiS<sub>6</sub>, Cu<sub>8</sub>GeS<sub>6</sub>, Ag<sub>8</sub>GeS<sub>6</sub> and Ag<sub>8</sub>SnS<sub>6</sub>

Cu eie d = 0.12	Compound	SHG coefficients (pm V <sup>-1</sup> )	$VE (pm V^{-1})$	VH (pm V <sup>-1</sup> )
$Cu_8SIS_6$ $d_{33} = -8.13$ $-5.20$ $-2.93$ $Cu_8GeS_6$ $d_{33} = 11.03$ $1.72$ $9.31$ $Ag_8GeS_6$ $d_{33} = -4.98$ $-7.98$ $3.0^1$ $Ag_8SnS_6$ $d_{33} = 5.78$ $-2.21$ $7.99$	Ag <sub>8</sub> GeS <sub>6</sub>	$d_{33} = -4.98$	−7 <b>.</b> 98	$3.0^{1}$

contributor and Cu atoms have a part contribution. In Cu<sub>8</sub>GeS<sub>6</sub> (Fig. 3c and d), the occupied states are mainly decided by Cu atoms. S and Cu atoms together contribute to the unoccupied states and Ge atoms have little contribution. The situation is consistent with the PDOS of Cu<sub>8</sub>SiS<sub>6</sub> and Cu<sub>8</sub>GeS<sub>6</sub> (Fig. 2a and b), which also illustrates that [CuS] groups mainly determine the SHG response.

As for Ag<sub>8</sub>GeS<sub>6</sub>, the VE process has a positive effect on the largest SHG coefficient ( $d_{33}$ ), however, on the contrary, the VH process has a positive effect on the largest SHG tensor  $(d_{33})$  for Ag<sub>8</sub>SnS<sub>6</sub>. So, here, we analyse the VE of Ag<sub>8</sub>GeS<sub>6</sub> (Fig. 3e and f) and VH of Ag<sub>8</sub>SnS<sub>6</sub> (Fig. 3g and h), respectively. In the VE process of Ag<sub>8</sub>GeS<sub>6</sub>, it clearly shows that not only Ag atoms contribute to the SHG effect, but also the contribution of S atoms is appreciable and intense. However, in Ag<sub>8</sub>SnS<sub>6</sub>, the VH process is dominant, and Ag atoms mainly dominate the occupied states. In the unoccupied states, the contribution is mainly from Ag and S atoms. So, we can draw a conclusion that [AgS] groups mainly contribute to the SHG effect in Ag<sub>8</sub>GeS<sub>6</sub> and Ag<sub>8</sub>SnS<sub>6</sub>. Similar

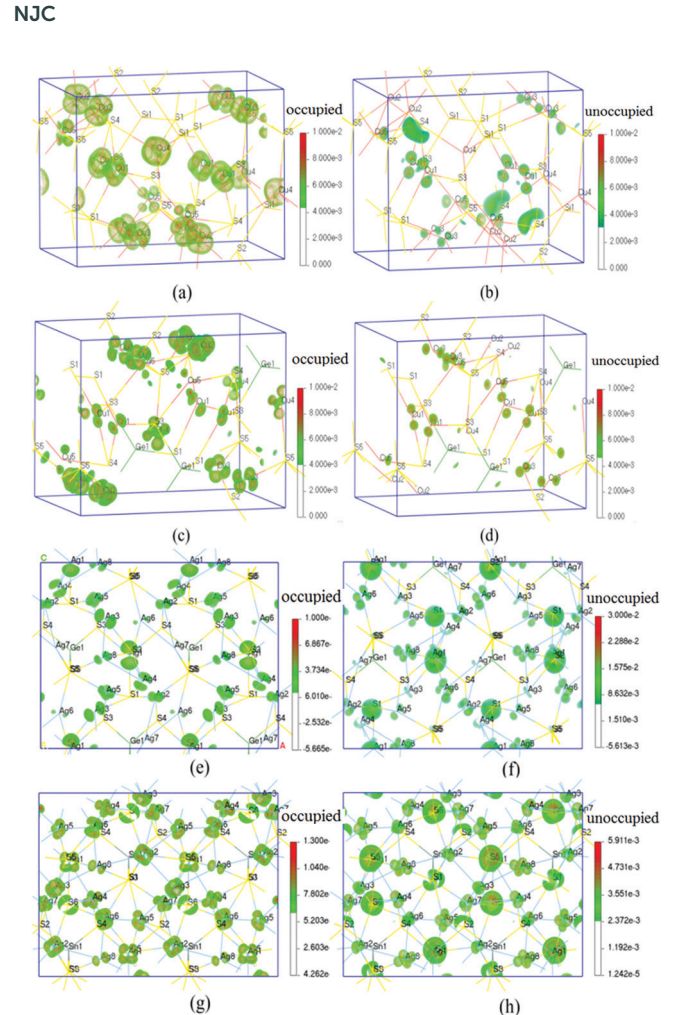


Fig. 3 SHG-density of VE state for  $Cu_8SiS_6$  (a and b), VH state for  $Cu_8GeS_6$  (c and d), VE state for  $Ag_8GeS_6$  (e and f), and VH state for  $Ag_8SnS_6$  (g and h).

results were also obtained from the electronic band structures of Ag<sub>8</sub>GeS<sub>6</sub> and Ag<sub>8</sub>SnS<sub>6</sub> (Fig. 2c and d).

The strong covalency will lead to a larger SHG effect, and the calculated Mulliken population results revealed that the covalency of the B-site atom and S is stronger than that of the A-site atom and S (shown in Table S3, ESI†). But, on the contrary, it is curious to find that A-site cations (d¹⁰ Cu and d¹⁰ Ag) have a more intense effect on the SHG responses; it is a little bit unusual that B-site cation groups ([GeS₄], [SnS₄] and [SiS₄]) have a minor contribution to the SHG effect, which is coincident with the dipole moment calculation results (shown in Table S2, ESI†). <sup>45</sup> In Cu<sub>8</sub>SiS<sub>6</sub>, it is clearly shown that the dipole moment of the [CuS] group is larger than that of the [SiS₄] group, and the situation in Cu<sub>8</sub>GeS<sub>6</sub> is the same as that in Cu<sub>8</sub>SiS<sub>6</sub>. As for Ag<sub>8</sub>GeS<sub>6</sub> and Ag<sub>8</sub>SnS<sub>6</sub>, the value of the dipole moment of the [AgS] group is larger than that of the [GeS] group and [SnS] group.

Although all title compounds have the similar formula  $A_8BC_6$ , it is interesting to note that the largest SHG coefficients have an apparent difference between  $Cu_8SiS_6$  ( $d_{33}=-8.13$  pm  $V^{-1}$ ),  $Cu_8GeS_6$  ( $d_{33}=11.03$  pm  $V^{-1}$ ),  $Ag_8SnS_6$  ( $d_{33}=5.78$  pm  $V^{-1}$ ) and  $Ag_8GeS_6$  ( $d_{33}=-4.98$  pm  $V^{-1}$ ). By analysing the PDOS of all compounds (Fig. 2), it is clear that the dp hybridization between

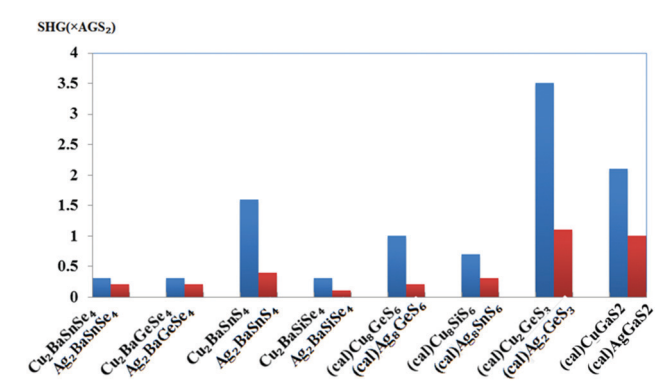


Fig. 4 Comparison of SHG response among the  $A_2BaBQ_4$  system, the  $A_8BS_6$  system and the  $N_2GeS_3$  system. A = Cu and Ag; B = Si, Ge, and Sn; Q = S and Se.

Cu ( $Cu_8GeS_6$  and  $Cu_8SiS_6$ ) and S is more intense than the dp hybridization between Ag ( $Ag_8GeS_6$  and  $Ag_8SnS_6$ ) and S from -3 eV to the Fermi level at the valence band top. We have also summarized the SHG effect of ternary and quaternary infrared materials containing Ag and Cu (shown in Fig. 4), noting that the SHG effect shows a decreasing tendency from Cu to Ag, and this is also because the dp hybridization between Cu and S is more intense than Ag and S. That is why the SHG effect of all title compounds behaves differently.

### Conclusion

In summary, the electronic structures and optical properties of the Ag/Cu containing chalcogenides have been calculated by the DFT method. We concluded that the B-site ion size, compound volume size and dp hybridization induce the changes of the band gap. The moderate birefringences in these chalcogenide compounds imply that they are phase-matching. By using the SHG-density method and dipole moment calculations, the contribution of respective ion and ion groups was explored. The SHG effect arises mainly from A-site cations and S groups, [CuS<sub>3</sub>] and [CuS<sub>4</sub>] in Cu<sub>8</sub>SiS<sub>6</sub> and Cu<sub>8</sub>GeS<sub>6</sub>, and [AgS<sub>2</sub>], [AgS<sub>3</sub>] and [AgS<sub>4</sub>] in Ag<sub>8</sub>GeS<sub>6</sub> and Ag<sub>8</sub>SnS<sub>6</sub>. While B-site cation groups, [GeS<sub>4</sub>], [SnS<sub>4</sub>] and [SiS<sub>4</sub>] have little contribution to the SHG responses of the ternary compounds mainly because they offset each other. It is also found that dp hybridization between Cu and S is more intense than Ag and S from -3 eV to the Fermi level at the top of the valence band, which clarifies the enhanced SHG effect from Ag<sub>8</sub>GeS<sub>6</sub> and Ag<sub>8</sub>SnS<sub>6</sub> to Cu<sub>8</sub>SiS<sub>6</sub> and Cu<sub>8</sub>GeS<sub>6</sub>. This study provides a feasible way to design and synthesize good-performance IR NLO materials.

#### Conflicts of interest

There are no conflicts to declare.

# Acknowledgements

This work is supported by the National Natural Science Foundation of China (Grant No. 11774414). MHL is grateful for the

database service provided by NCHC (Taiwan) and computer equipment donated by KeyWin Inc.

#### References

Paper

- 1 K. Wu, B. B. Zhang, Z. H. Yang and S. L. Pan, J. Am. Chem. Soc., 2017, 139, 14885-14888.
- 2 Z. G. Xia and K. R. Poeppelmeier, Acc. Chem. Res., 2017, 50, 1222.
- 3 H.-Y. Chang, S.-H. Kim, P. S. Halasyamani and K. M. Ok, J. Am. Chem. Soc., 2009, 131, 2426-2427.
- 4 J. S. Knyrim, P. Becker, D. Johrendt and H. Huppertz, Angew. Chem., Int. Ed., 2006, 45, 8239-8241.
- 5 S. Haussuhl, Z. Kristallogr. Cryst. Mater., 1964, 120, 401.
- 6 T. T. Tran, H. Yu, J. M. Rondinelli, K. R. Poeppelmeier and P. S. Halasyamani, Chem. Mater., 2016, 28, 5238-5258.
- 7 J. D. Bierlein and H. Vanherzeele, J. Opt. Soc. Am. B, 1989, 622-633.
- 8 C. T. Chen, B. C. Wu, A. D. Jiang and G. M. You, Sci. Sin. Ser. B, 1985, 28, 235-243.
- 9 C. T. Chen, Y. C. Wu, A. D. Jiang, B. C. Wu, G. M. You, R. K. Li and S. J. Lin, J. Opt. Soc. Am. B, 1989, 616-621.
- 10 F. Liang, L. Kang, Z. S. Lin and Y. C. Wu, Cryst. Growth Des., 2017, 17, 2254-2289.
- 11 M. Luo, Y. X. Song, C. S. Lin, N. Ye, W. D. Cheng and X. F. Long, Chem. Mater., 2016, 28, 2301-2307.
- 12 G. H. Yuan and D. F. Xue, Acta Crystallogr., Sect. B: Struct. Sci., 2007, 63, 353.
- 13 X. F. Wang, B. B. Zhang, F. F. Zhang, Z. H. Yang and S. L. Pan, Angew. Chem., Int. Ed., 2017, 14307-14311.
- 14 G. Q. Shi, Y. Wang, F. F. Zhang, B. B. Zhang, Z. H. Yang, X. L. Hou, S. L. Pan and K. R. Poeppelmeier, J. Am. Chem. Soc., 2017, 139, 10645-10648.
- 15 B. B. Zhang, G. Q. Shi, Z. H. Yang, F. F. Zhang and S. L. Pan, Angew. Chem., Int. Ed., 2017, 56, 3916-3919.
- 16 H. Wu, S. Pan, K. R. Poeppelmeier, H. Li, D. Jia, Z. Chen, X. Fan, Y. Yang, J. M. Rondinelli and H. Luo, J. Am. Chem. Soc., 2011, 133, 7786-7790.
- 17 X. Dong, Q. Jing, Y. Shi, Z. Yang, S. Pan, K. R. Poeppelmeier, J. Young and J. M. Rondinelli, J. Am. Chem. Soc., 2015, 137, 9417-9422.
- 18 Y. Wang, B. B. Zhang, Z. H. Yang and S. L. Pan, Angew. Chem., Int. Ed., 2018, 2172-2176.
- 19 A. O. Okorogu, S. B. Mirov, A. Y. Dergachev, W. Lee, D. I. Crouthamel, K. L. Vodopyanov, N. Jenkins and V. V. Badikov, Opt. Commun., 1998, 155, 307-312.
- 20 G. D. Boyd, H. M. Kasper, J. H. McFee and F. G. Storz, Quantum Electron., 1972, 8, 900-908.
- 21 G. H. Zou, L. Huang, N. Ye, C. S. Lin, W. D. Cheng and H. Huang, J. Am. Chem. Soc., 2013, 135, 18560-18566.

- 22 S. G. Zhao, P. F. Gong, L. Bai, X. Xu, S. Q. Zhang, Z. H. Sun, Z. S. Lin, M. C. Hong, C. T. Chen and J. H. Luo, Nat. Commun., 2014, 5, 4019.
- 23 L. Y. Nian, J. B. Huang, K. Wu, Z. Su, Z. H. Yang and S. L. Pan, RSC Adv., 2017, 7, 29378-29385.
- 24 L. y. Nian, K. Wu, G. J. He, Z. H. Yang and S. L. Pan, Inorg. Chem., 2018, 57, 3434-3442.
- 25 P. M. Levalois and G. Allais, Acta Crystallogr., Sect. C: Struct. Chem., 1981, 1816-1819.
- 26 M. Ishii, M. Onoda and K. Shibata, Solid State Ionics, 1999, 11-18.
- 27 D. I. Bletskan, Semicond. Phys., Quantum Electron. Optoelectron., 2017, 20, 19-25.
- 28 C.-L. Lu, L. Zhang, Y.-W. Zhang, S.-Y. Liu and Y. Mei, Chin. Phys. B, 2015, 24, 017501.
- 29 N. Wang, Neues Jahrb. Mineral., Monatsh., 1978, 269-272.
- 30 C. M. Huang, F. F. Zhang, B. B. Zhang, Z. H. Yang and S. L. Pan, New J. Chem., 2018, 42, 12091-12097.
- 31 A. H. Reshak, Eur. Phys. J. B, 2005, 47, 503-508.
- 32 A. M. Rappe, K. M. Rabe, E. Kaxiras and J. D. Joannopoulos, Phys. Rev. B: Condens. Matter Mater. Phys., 1990, 41, 1227-1230.
- 33 J. S. Lin., A. Qteish, M. C. Payne and V. Heine, Phys. Rev. B: Condens. Matter Mater. Phys., 1993, 47, 4174-4180.
- 34 B.-H. Lei, Z. H. Yang, H. W. Yu, C. Cao, Z. Li, C. Hu, K. R. Poeppelmeier and S. L. Pan, J. Am. Chem. Soc., 2018, 10726-10733.
- 35 C. Hu, B. Zhang, B.-H. Lei, S. Pan and Z. Yang, ACS Appl. Mater. Interfaces, 2018, 10, 26413-26421.
- 36 Z. Zhang, Y. Wang, B. Zhang, Z. Yang and S. Pan, Angew. Chem., Int. Ed., 2018, 57, 6577-6581.
- 37 Z. H. Yang, C. Hu, M. Mutailipu, Y. Z. Sun, K. Wu, M. Zhang and S. L. Pan, J. Mater. Chem. C, 2018, 6, 2435-2442.
- 38 C. D. Gelatt, A. R. Williams and V. L. Moruzzi, Phys. Rev. B: Condens. Matter Mater. Phys., 1983, 27, 2005-2013.
- 39 J. N. Cheng, M.-H. Lee and J. Zhang, J. Alloys Compd., 2018, 768, 883-888.
- 40 M.-H. Lee, C.-H. Yang and J.-H. Jan, Phys. Rev. B: Condens. Matter Mater. Phys., 2004, 70, 155-163.
- 41 Z. Li, Q. Liu, Y. Wang, T. Iitaka, H. Su, T. Tohyama, Z. H. Yang and S. L. Pan, Phys. Rev. B: Condens. Matter Mater. Phys., 2017, 96, 035205.
- 42 B. H. Lei, Z. H. Yang and S. L. Pan, Chem. Commun., 2017, 53, 2818-2821.
- 43 M. Mutailipu, M. Zhang, B. Zhang, L. Wang, Z. Yang, X. Zhou and S. Pan, Angew. Chem., Int. Ed., 2018, 57, 6095-6099.
- 44 H. Li, G. M. Li, K. Wu, B. B. Zhang, Z. H. Yang and S. L. Pan, Chem. Mater., 2018, 30, 7428-7432.
- 45 G. M. Li, K. Wu, Q. Liu, Z. H. Yang and S. L. Pan, J. Am. Chem. Soc., 2016, 138, 7422-7428.